

RESEARCH

Open Access



Predicting placenta accreta spectrum and high postpartum hemorrhage risk using radiomics from T2-weighted MRI

Jinli Zou¹, Wei Wei², Yingzhen Xiao², Xinlian Wang¹, Keyang Wang¹, Lizhi Xie³ and Yuting Liang^{1*}

Abstract

Background Antenatal diagnosis of placenta accreta spectrum (PAS) is of critical importance, considering that women have much better outcomes when delivery occurs at a level III or IV maternal care facility before labor initiation or bleeding, thus avoiding placental disruption. Herein, we aimed to investigate the performance of magnetic resonance imaging (MRI) in antenatal prediction of PAS and postpartum hemorrhage (PPH).

Methods This retrospective study included 433 women with singleton pregnancies (PAS group, $n=208$; non-PAS group, $n=225$; PPH-positive (PPH (+)) group, $n=80$; PPH-negative (PPH (-)) group, $n=353$), who were randomly divided into a training set and a test set in a 7:3 ratio. Radiomic features were extracted from T2WI (T2-weighted imaging). Features strongly correlated with PAS and PPH ($p < 0.05$) were selected using Pearson correlation, followed by LASSO regression for dimensionality reduction. Subsequently, radiomics models were constructed for PAS and PPH risk prediction, respectively. Regression analyses were conducted using radiomics score (R-score) and clinical factors to identify independent clinical risk factors for PAS and PPH, leading to the development of corresponding clinical models. Next, clinical-radiomics models were built by combining R-score and clinical risk factors. The predictive performance of the models was evaluated using nomograms, calibration curves, and decision curves.

Results The clinical-radiomics models and radiomics models for predicting PAS and PPH risk both outperformed their clinical models in the training and testing sets. For PAS, the AUC (Area Under the Receiver Operating Characteristic Curve) of the clinical-radiomics model, radiomics model, and clinical model in the training set are 0.918, 0.908, and 0.755, respectively, and in the testing set, the AUCs are 0.885, 0.866, and 0.771, respectively. For PPH, the AUCs of the clinical-radiomics model, radiomics model, and clinical model in the training set are 0.918, 0.884, and 0.723, respectively, and in the testing set, the AUCs are 0.905, 0.860, and 0.688, respectively. The DeLong test p-values between the clinical-radiomics models and radiomics models for predicting PAS and PPH are both less than 0.05. Additionally, in the testing set, the clinical-radiomics models perform best in predicting PAS and PPH risk, with accuracies of 82.31% and 84.61%, respectively.

Jinli Zou, Wei Wei and Yingzhen Xiao should be considered co-first authors.

*Correspondence:

Yuting Liang
liangyuting@cmmu.edu.cn

Full list of author information is available at the end of the article



© The Author(s) 2025. **Open Access** This article is licensed under a Creative Commons Attribution-NonCommercial-NoDerivatives 4.0 International License, which permits any non-commercial use, sharing, distribution and reproduction in any medium or format, as long as you give appropriate credit to the original author(s) and the source, provide a link to the Creative Commons licence, and indicate if you modified the licensed material. You do not have permission under this licence to share adapted material derived from this article or parts of it. The images or other third party material in this article are included in the article's Creative Commons licence, unless indicated otherwise in a credit line to the material. If material is not included in the article's Creative Commons licence and your intended use is not permitted by statutory regulation or exceeds the permitted use, you will need to obtain permission directly from the copyright holder. To view a copy of this licence, visit <http://creativecommons.org/licenses/by-nc-nd/4.0/>.

Conclusion This novel clinical-radiomics model has a robust performance in predicting PAS antepartum and predicting massive PPH in pregnancies.

Keywords Placenta accreta spectrum, Postpartum hemorrhage, Magnetic resonance imaging, Radiomics

Introduction

Placenta accreta spectrum (PAS) is a morbid pregnancy condition characterized by abnormal placental adherence and invasion into the uterine wall, and may result in postpartum hemorrhage (PPH), hysterectomy, and even maternal mortality [1, 2]. In recent years, the incidence of PAS has increased significantly, from approximately 0.02% of pregnancies in the 1970s to 0.17% in recent years. This rise is primarily driven by the increasing cesarean delivery rate, along with factors such as advanced maternal age and the use of in vitro fertilization [3–5].

PPH, defined as >500 mL estimated blood loss (EBL) during vaginal or >1000 mL EBL during cesarean delivery, is an important factor in maternal morbidity and mortality [6]. Therefore, accurately identifying PAS patients antenatally and predicting the risk of maternal EBL \geq 1500 mL can be used to classify these women as high risk for PPH (+); those with an EBL risk of <1500 mL can be classified as low-risk for PPH (-). Transferring PPH(+) patients from institutions lacking multidisciplinary management capabilities to those institutions with multidisciplinary treatment capabilities, along with early warning and the formulation of comprehensive treatment plans, is of crucial importance in reducing severe adverse pregnancy outcomes and ensuring the safety of both mother and child [5].

Patients with PAS are often asymptomatic or have low-specificity symptoms antenatally, resulting in approximately half of cases remaining undiagnosed, with detection rates ranging from 30–53% [7–9]. The most crucial step in identifying patients at risk for PAS is evaluating their clinical and obstetric profile. The absence of ultrasound findings or negative ultrasound results does not exclude PAS [10, 11]. Although ultrasound is the first-line examination for diagnosing PAS [12], its detection rate is significantly reduced or even impossible in cases where the placenta is located in the posterior wall or fundus of the uterus, or when imaging is compromised by amniotic fluid, maternal obesity, or intestinal gas [13, 14].

MRI serves as a valuable complementary tool to ultrasound due to its excellent soft tissue resolution and ability to evaluate placental invasion depth, attachment location, and relationships with adjacent structures, independent of maternal body size, intestinal gas, or placental location [15, 16]. Additionally, T2WI excels in visualizing placental heterogeneity, particularly intensity inhomogeneity caused by placental maturation or pathology [17].

However, its diagnostic accuracy may be limited by the subjectivity of radiologist. The integration of MRI with radiomics, which extracts high-throughput image features invisible to the naked eye, is expected to improve diagnostic precision and support individualized treatment planning [18–24].

Based on placental MRI images, this study utilized radiomics to establish models for the accurate antenatal diagnosis of PAS and prediction of PPH risk. The PAS prediction model aims to identify whether a pregnant woman has PAS, while the PPH risk prediction model focuses on assessing the risk of severe PPH. These models may facilitate early identification of high-risk groups, guide clinical risk stratification, optimize intraoperative hemorrhage management, and improve maternal and neonatal outcomes.

Materials and methods

Study population

This retrospective analysis included singleton pregnant women suspected of PAS who underwent antenatal MRI in Beijing Obstetrics and Gynecology Hospital between January 2018 and June 2023 and were hospitalized for delivery at an elective time. The inclusion criteria were: (1) patients with singleton pregnancies who were clinically suspected of PAS (based on placental abnormalities identified by ultrasound examination and/or high-risk clinical factors) and underwent MRI; (2) patients whose gestational age was \geq 21 weeks; (3) patients with complete records of delivery surgery, postoperative diagnosis and/or pathological diagnosis. The exclusion criteria were as follows: (1) MRI images with severe artifacts and poor image quality due to fetal movement or other reasons; (2) pregnant women whose pregnancy resulted in stillbirth; (3) The patient's key clinical information is missing more than 30%. Finally, singleton pregnant patients meeting the inclusion and exclusion criteria were randomly allocated to the training set ($n = 303$) and the test set ($n = 130$) in a 7:3 ratio using a randomized sampling approach.

This retrospective study was approved by the Ethics Committee of Beijing Obstetrics and Gynecology Hospital Affiliated with Capital Medical University (approval number: 2022-KY-049-01). The study was conducted according to the principles of the Declaration of Helsinki. The Ethics Committee of Beijing Obstetrics and Gynecology Hospital Affiliated with Capital Medical University has waived the need for informed consent.

MRI protocols

Data were acquired using a GE Discovery 750 3.0T MRI scanner with a phase-array body coil. A pelvic positioning scan was performed in the supine position with the feet first, followed by axial, sagittal, and coronal scans according to the position of the placenta using non-contrast imaging (plain scan). T2WI images were sequentially collected with a single-shot fast spin echo (SSFSE) sequence and fast imaging employing a steady-state acquisition (FIESTA) sequence. The parameters of MRI sequences are presented in Supplementary Table S1.

PAS diagnostic and typing criteria

The following criteria were used for intraoperative and postoperative pathological examination [25]: (1) non-PAS: the placenta can be delivered by itself; (2) PA: the placenta has to be removed manually, and the pathology shows that the villi are in contact with the surface of the myometrium but have not invaded the myometrium; (3) PI: significant amounts of hypervascularity, and the pathology shows that the villi have invaded the myometrium but did not penetrate the plasma membrane layer; (4) PP: invasion of placental villi into the muscularis propria, up to the plasma layer and even into the adjacent pelvic tissues.

Image segmentation and feature extraction

The study flowchart is presented in Fig. 1. The original SSFSE-T2WI images were imported into ITK-SNAP software (v3.6.0, www.itksnap.org). The placenta region

(including the myometria) was manually sketched layer by layer on all sequence images by a resident physician (Physician 1) with 1-year experience in MRI diagnosis of gynecological and obstetric diseases. Validation was done by another associate chief physician (Physician 2) with > 10 years of experience, and the region of interest (ROI) were saved. Figure 2 (a, c) is two examples of original MRI images, and Fig. 2 (b, d) illustrates the labeled ROI area on MRI images. Another attending physician with 8 years of working experience (physician 3) randomly selected 70 cases to independently delineate the ROI of the placenta (including myometrium), as shown in Fig. 2 (b, d). We used the intraclass correlation coefficient (ICC) as the consistency evaluation metric to assess the consistency in the ROI delineation process among the three doctors. An ICC value of > 0.8 indicated good consistency.

The radiomic features were then extracted using the pyradiomics library (v 3.1.0, <https://pyradiomics.readthedocs.io>). Pyradiomics is a widely used medical imaging analysis tool known for its mature algorithms and stable performance. It can extract a wide range of radiomic features, including first-order statistical features, shape features, texture features, and wavelet-based features, thus ensuring the comprehensiveness and accuracy of the features used in our study. The feature extraction was performed in a Python 3.7.4 environment.

Feature selection

In this study, feature selection and model construction were conducted using R software (v 3.6.1, www.r-project.org).

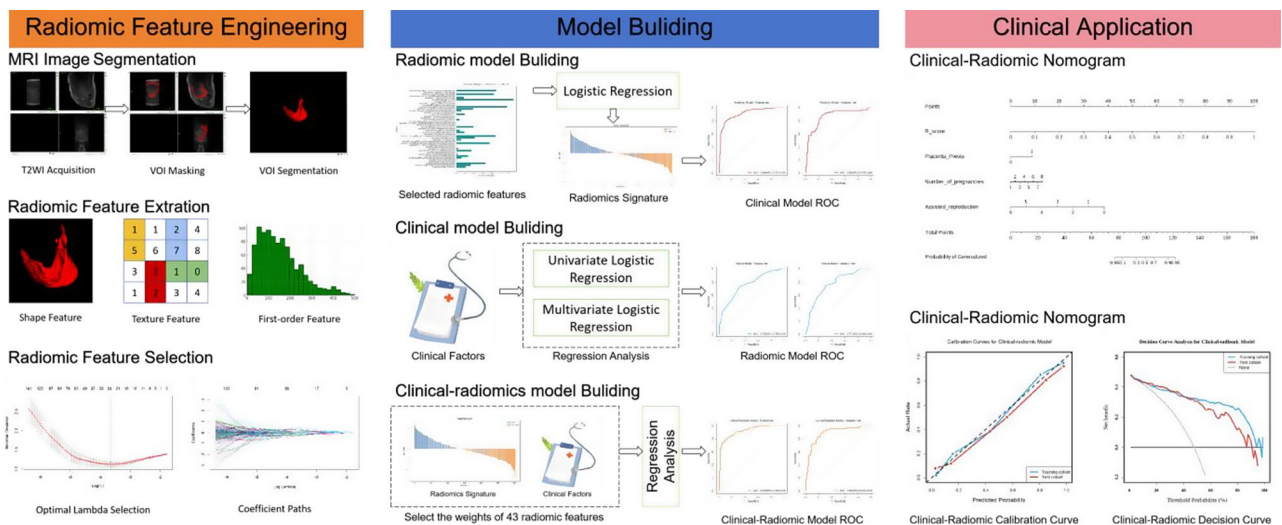


Fig. 1 This study includes radiomic feature engineering, model construction, and clinical application. The ROI representing the placenta and adjacent uterine tissues was delineated, from which 806 radiomic features were extracted. The least absolute shrinkage and selection operator (LASSO) was then used to select radiomic features associated with the target variables (the presence or absence of PAS and the risk level (high or low) of PPH). Based on the selected features, a radiomics signature was constructed using a logistic regression classifier, referred to as the radiomics model. Univariate and multivariate analyses were performed to screen for clinically independent risk factors, and a clinical model was developed based on these factors. The clinical and radiomic features were combined to construct a clinical radiomics model. The performance of the three models was compared to select the optimal prediction model. Finally, the performance and clinical value of the optimized model were validated through calibration and decision curve analysis

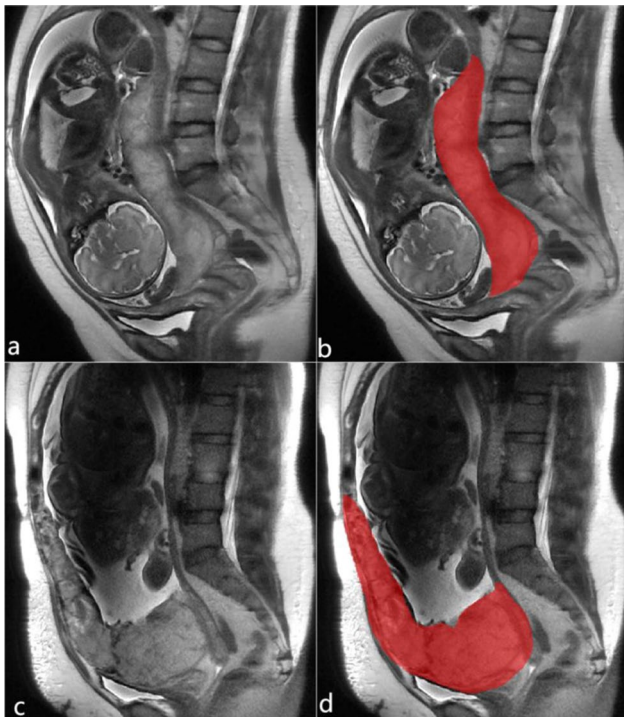


Fig. 2 Representative cases and delineation of ROI. **(a, b)** A 37-year-old woman at 32 gestation weeks with placenta previa. She had a history of G2P1 with one previous cesarean delivery. She had an EBL of 700 mL during cesarean delivery. Based on the clinical-radiomics model, the predicted radiomics score was 0.0508; she was classified as having a low risk of PPH. **(c, d)** A 33-year-old woman at 36 gestation weeks with placenta previa. She had a history of G1P1 with one previous cesarean delivery. She had an EBL of 6600 mL during cesarean delivery. Based on the clinical-radiomics model, the predicted R-score was 0.9130; she was classified as having a high risk of PPH

org). First, Pearson correlation coefficients were calculated for each feature in relation to the target variable (the presence or absence of PAS and the risk of PPH [high or low]). Features with a P-value > 0.05 were excluded, retaining only those with a statistically significant linear correlation with the target variable. To further enhance the predictive accuracy and prevent overfitting of the model, features with an absolute Pearson correlation coefficient > 0.2 were then selected, ensuring a stronger correlation with the target variable. Finally, the ten-fold cross-validated Least Absolute Shrinkage and Selection Operator (LASSO) regression method was applied to further refine the feature set.

Models construction

Based on the selected radiomic features, this study utilized a logistic regression algorithm with strong interpretability to develop the radiomics model, which generates regression coefficients and odds ratios to quantify the contribution of individual features to the target variable. In addition, univariate and multifactor logistic regression analyses were used to screen out clinically independent

risk factors related to target variables for clinical factors. Clinical models were constructed, and R-score was combined with clinically independent risk factors based on the output of radiomics models to construct a clinical-radiomics model. Therefore, we constructed clinical, radiomics, and clinical-radiomics models for predicting PAS and the risk of PPH in patients suspected of PAS.

Model validation and evaluation

In this study, the predictive performance of different models (clinical, radiomics, and clinical-radiomics) for PAS and PPH was evaluated using ROC curves and AUC. ROC curves were plotted based on the prediction results, and a series of comprehensive metrics, including AUC, sensitivity, specificity, accuracy, and positive and negative predictive values, were calculated to assess model performance. The optimal threshold for each model was determined by selecting the value corresponding to the maximum Youden Index derived from the ROC curve of the training set. Cases with a predicted probability of PAS equal to or exceeding this threshold were classified as positive, while those below the threshold were classified as negative. Similarly, cases with a predicted probability of PPH risk equal to or exceeding the threshold were categorized as PPH (+), whereas those below the threshold were categorized as PPH (-). A clinically usable visual nomogram was constructed for the clinical radiomics model. A calibration curve was plotted to explore the predictive accuracy of the nomogram. Decision curve analysis (DCA) was employed to determine the value of the nomogram at different clinical decision thresholds.

Statistical analysis

Statistical analyses were performed using R software (version 3.6.1, www.r-project.org) and SPSS (version 22.0; IBM Corp). Missing data for continuous and categorical variables were handled using mean and mode imputation, respectively. Continuous variables are presented as medians and interquartile ranges (IQRs). Qualitative variables are presented as frequencies and percentages. Continuous variables were compared using the independent samples t-test, while categorical variables were analyzed using the chi-square test. Univariate and multivariate logistic regression analyses were used to calculate the p-values, ratios (ORs) and their 95% confidence intervals (CIs) for each clinical factor and R-score in relation to the target variables (the presence or absence of PAS and the risk of PPH [high or low]). Factors with p-values < 0.05 in both univariate and multivariate analyses were identified as independent clinical risk factors for PAS and the risk levels of PPH. The DeLong test was used to analyze whether there was a significant difference between the radiomics and clinical-radiomics models.

Results

Clinical characteristics of patients

Following the application of inclusion and exclusion criteria, 433 pregnant women (aged 23–46 years) suspected

Table 1 Clinical characteristics of patients in training set and test set

Characteristics	Training set (n = 303)	Test set (n = 130)	Statistical value	P-value
Maternal Age, years	34(23–45)	34(23–46)	-0.64	0.522 [ⓐ]
Gestational age at MRI, weeks	33(22–40)	33(21–39)	-0.453	0.65 [ⓐ]
Placenta Previa			0	1 [ⓐ]
Positive	191 (63.04)	82 (63.08)		
Negative	112 (36.96)	48 (36.92)		
Prior cesarean deliveries, times			3.96	0.266 [ⓐ]
0	166(54.79)	65(50)		
1	101(33.33)	49(37.69)		
2	30(9.90)	16(12.31)		
3	6(1.98)	0(0)		
Gravidities, times			2.367	0.5 [ⓐ]
0	0(0)	0(0)		
1	64(21.12)	27(20.77)		
2	90(29.71)	32(24.62)		
3	63(20.79)	35(26.92)		
> 3	86(28.38)	36(27.69)		
Parities, times			5.893	0.207 [ⓐ]
0	135(44.55)	54(41.54)		
1	128(42.24)	59(45.38)		
2	33(10.89)	16(12.31)		
3	7(2.31)	0(0)		
> 3	0(0)	1(0.77)		
History of abortion, times			5.503	0.239 [ⓐ]
0	149(49.17)	57(43.85)		
1	79(26.07)	41(31.54)		
2	45(14.85)	18(13.85)		
3	20(6.60)	5(3.85)		
> 3	10(3.30)	9(6.92)		
History of other uterine operations, times			5.641	0.228 [ⓐ]
0	246(81.19)	97(74.62)		
1	47(15.51)	22(16.92)		
2	6(1.98)	7(5.38)		
3	3(0.99)	3(2.31)		
> 3	1(0.33)	1(0.77)		
Assisted reproduction, times			1.142	0.888 [ⓐ]
0	265(87.46)	118(90.77)		
1	29(9.57)	9(6.92)		
2	2(0.66)	1(0.77)		
3	3(0.99)	1(0.77)		
> 3	4(1.32)	1(0.77)		

Note:[ⓐ] indicates that the data are in median (range) format and the statistic is a t-value. [ⓑ] indicates that the data are in number (percentage) format and the statistic is a chi-square value. PAS: placenta accreta spectrum

of PAS were enrolled in this retrospective study. Based on the study design, the cohort was divided into training and test sets. Comparative analysis of clinical characteristics between the two sets, conducted using t-tests and chi-square tests, revealed no significant differences ($P > 0.05$), confirming their comparability (Table 1).

Analysis of clinical differences between study groups

In this study, patients were stratified into two groups based on distinct research objectives: PAS vs. Non-PAS, and PPH (+) vs. PPH (-). Clinical characteristics were compared between groups using t-tests and chi-square tests. Significant differences ($P < 0.05$) between PAS and Non-PAS groups were observed in gestational age at MRI, placenta previa, prior cesarean deliveries, gravidities, parities, and assisted reproduction, suggesting potential associations with PAS (Table S2). Similarly, significant differences ($P < 0.05$) between PPH (+) and PPH (-) groups were noted in gestational age at MRI, placenta previa, prior cesarean deliveries, gravidities, and parities, indicating possible links to PPH (Table S3).

Consistency assessment

Excellent inter-observer agreement was demonstrated for ROI annotation reproducibility among the annotators (Physician 1 and Physician 2, Physician 2 and Physician 3). The intraclass correlation coefficient (ICC) for ROI annotation consistency between Physician 1 and Physician 2 ranged from 0.81 to 0.91, while the ICC for the 70 randomly selected ROI annotations validated by Physician 2 and Physician 3 ranged from 0.83 to 0.97, indicating high reproducibility.

Features selection and model construction

A total of 806 radiomic features were extracted from T2WI. After feature screening through Pearson correlation coefficient analysis and LASSO regression, it was found that 43 radiomic features were highly associated with PAS (Fig. 3A), and 31 radiomic features were highly associated with the risk of PPH (Fig. 3B). Based on the selected features, a logistic regression model was established to calculate the R-score:

$$R - score = \beta_0 + \beta_1 X_1 + \beta_2 X_2 + \dots + \beta_n X_n$$

where β_0 represents the truncation value of the best parameter λ , X_n represents the screened radiomic features, and β_n represents the coefficient β corresponding to the radiomic features. The R-score for each pregnant woman in the training and test sets for predicting PAS and PPH risk are shown in Fig. 4.

We conducted univariate and multivariate logistic regression analyses on clinical factors (such as maternal age, gestational age at MRI, gravidities, parities, prior cesarean deliveries, placenta previa, history of miscarriage, and assisted reproduction) as well as the scores

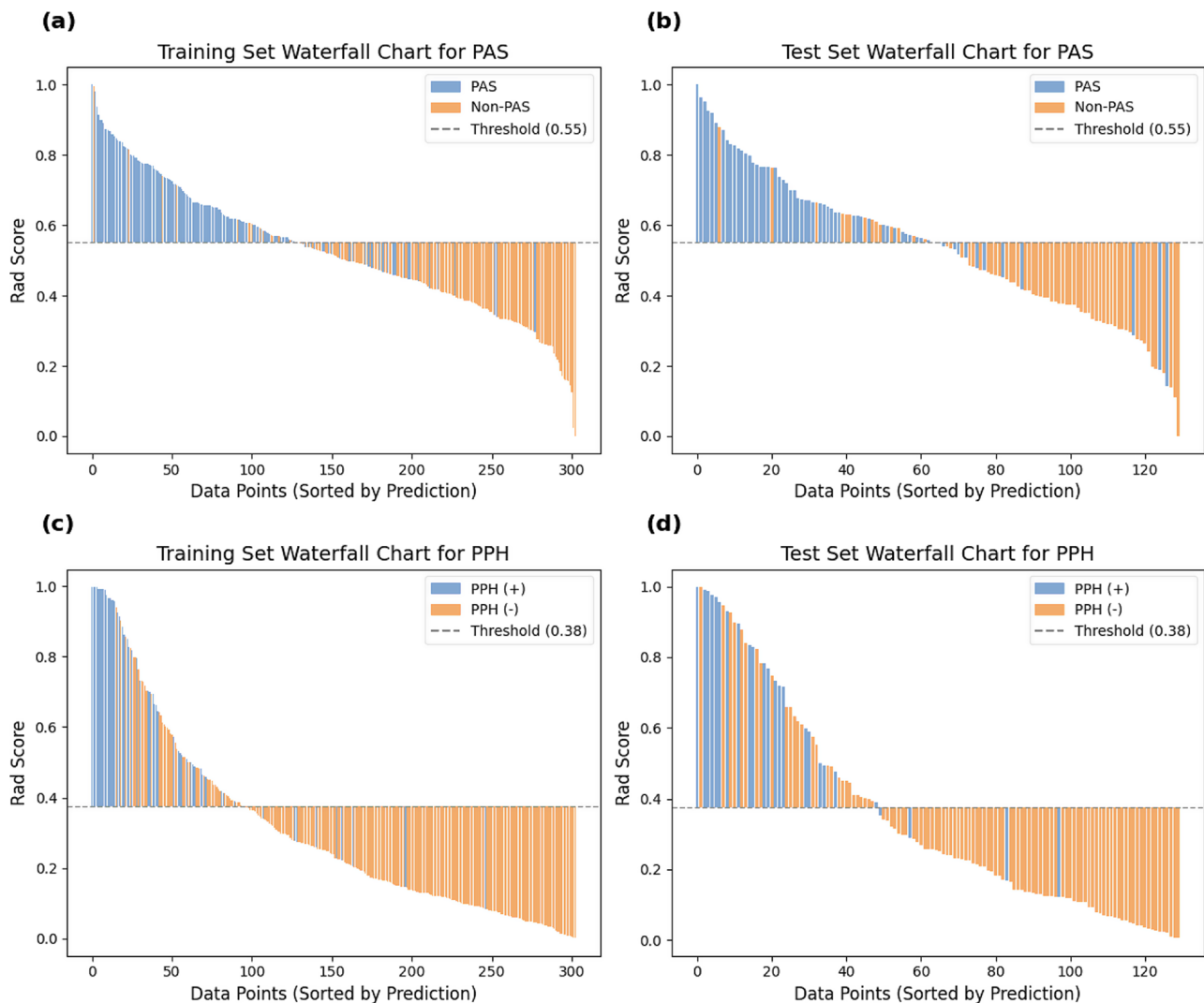


Fig. 4 Waterfall plots. **(a, b)** Histograms of radiomic features for predicting PAS in the training and test sets. Samples with PAS are represented by blue bars, and samples without PAS (Non-PAS) are represented by orange bars. The y-axis displays the values of the R-score. **(c, d)** Histograms of radiomic features for predicting PPH risk in the training and test sets. Samples with PPH (+) are represented by blue bars, and samples with PPH(-) are represented by orange bars. The y-axis displays the values of the R-score

($z=2.3696$, $P<0.05$), which showed a significant difference in performance between the combined clinical-radiomics model and the radiomics model for predicting PAS and for predicting the risk of PPH.

Clinical applications of clinical-radiomics models

Constructing a clinical-radiomics model into a nomogram can transform the output of a complex model into an intuitive probability score. Figure 7A presents the nomogram of the clinical-radiomics model for predicting PAS, where placenta previa, R-score, assisted reproduction, and gravidity are the input variables, indicating their significant predictive value for PAS. Figure 7B shows the nomogram of the clinical-radiomics model for predicting the risk of PPH, with placenta previa and R-score as the input variables, indicating their significant predictive

value for assessing the risk of PPH. The decision benefits of the models were quantified by Decision Curve Analysis (DCA), which revealed the clinical benefits predicted by the models at different thresholds. Figure 8A shows the decision curve of the clinical-radiomics model for predicting PAS, and Fig. 8B shows the decision curve of the clinical-radiomics model for predicting the risk of PPH. The results showed that the models demonstrated significant predictive benefits at multiple clinical decision thresholds. In addition, the predictive accuracy of the models was further confirmed by calibration curve analysis. Figure 9A shows the calibration curve of the clinical-radiomics model for predicting PAS, and Fig. 9B shows the calibration curve of the clinical-radiomics model for predicting the risk of PPH. The calibration curve analysis showed that the model predictions were

Table 2 Results of univariate and multivariate logistic regression analysis of predicting PAS

Characteristics	Univariate logistic regression analysis		Multivariate logistic regression analysis	
	OR (95% CI)	P value	OR (95% CI)	P value
R-score	1.178e+06 (5.074e+04–2.738e+07)	<0.001*	3.641e+05 (1.142e+04–1.161e+07)	<0.001*
Maternal Age	1.009 (0.954–1.067)	0.756	0.994 (0.910–1.086)	0.902
Gestational age at MRI	0.917 (0.854–0.986)	0.019*	1.068 (0.952–1.198)	0.263
Gravidities	1.499 (1.270–1.770)	<0.001*	3.069 (1.354–6.955)	0.007*
Parities	2.741 (1.916–3.920)	<0.001*	0.737 (0.228–2.386)	0.611
Prior cesarean deliveries	2.906 (2.011–4.200)	<0.001*	0.992 (0.381–2.583)	0.986
Placenta Previa	3.622 (2.194–5.979)	<0.001*	4.699 (2.051–10.763)	<0.001*
History of abortion	0.991 (0.825–1.191)	0.923	0.321 (0.135–0.763)	0.010*
History of other uterine operations	1.068 (0.788–1.448)	0.67	2.550 (1.411–4.610)	0.002*
Assisted reproduction	0.484 (0.274–0.852)	0.012*	0.307 (0.111–0.845)	0.022*

Note: * indicates that the variable has a p-value of less than 0.05 in univariate or multivariate analyses and satisfies the characteristic retention condition. The odds ratio (OR) indicates the degree of influence of an independent variable on the probability of the outcome. An OR > 1 suggests that the factor increases the likelihood of the outcome, while an OR < 1 indicates a reduced likelihood. The 95% confidence interval (CI) reflects the precision of the estimate; if the interval does not include 1, the effect is considered statistically significant ($p < 0.05$)

Abbreviations: OR, odds ratio; R-score, radiomics model output score

Table 3 Results of univariate and multivariate logistic regression analysis of predicting PPH risk

Characteristics	Univariate logistic regression analysis		Multivariate logistic regression analysis	
	OR (95% CI)	P value	OR (95% CI)	P value
R-score	3.863e+02 (9.1301–1.6348e+03)	<0.001*	5.376e+02 (7.526–3.840e+03)	<0.001*
Maternal Age	0.958 (0.890–1.031)	0.251	0.928 (0.824–1.045)	0.218
Gestational age at MRI	0.904 (0.828–0.986)	0.023	0.903 (0.785–1.038)	0.15
Gravidities	1.405 (1.177–1.677)	<0.001*	0.798 (0.371–1.716)	0.564
Parities	2.605 (1.763–3.848)	<0.001*	1.431 (0.235–8.708)	0.697
Prior cesarean deliveries	2.878 (1.955–4.237)	<0.001*	2.743 (0.613–12.271)	0.187
Placenta Previa	2.112e+01 (5.035–8.8609e+01)	<0.001*	4.019e+01 (6.459–2.501e+02)	<0.001*
History of abortion	1.164 (0.938–1.444)	0.169	1.874 (0.906–3.879)	0.091
History of other uterine operations	0.699 (0.423–1.155)	0.162	2.065 (1.088–3.921)	0.027*
Assisted reproduction	0.275 (0.069–1.094)	0.067*	0.289 (0.064–1.297)	0.105

Note: * indicates that the variable has a p-value of less than 0.05 in univariate or multivariate analyses and satisfies the characteristic retention condition. The odds ratio (OR) indicates the degree of influence of an independent variable on the probability of the outcome. An OR > 1 suggests that the factor increases the likelihood of the outcome, while an OR < 1 indicates a reduced likelihood. The 95% confidence interval (CI) reflects the precision of the estimate; if the interval does not include 1, the effect is considered statistically significant ($p < 0.05$)

Abbreviations: OR, odds ratio; R-score, radiomics model output score

Table 4 Model performance metrics

Variable	Model	Set	AUC	Accuracy	Sensitivity	Specificity	PPV	NPV
PAS	Clinical	Training set	0.755(95% CI, 0.700–0.810)	69.97%	74.48%	65.82%	66.67%	74%
		Test set	0.771(95% CI, 0.690–0.846)	72.31%	74.60%	70.15%	70.15%	74.60%
	Radiomics	Training set	0.908(95% CI, 0.873–0.941)	84.49%	81.37%	87.34%	85.51%	83.64%
		Test set	0.866(95% CI, 0.796–0.926)	81.53%	87.30%	76.12%	77.46%	86.44%
PPH	Clinical	Training set	0.918(95% CI, 0.886–0.945)	84.16%	80.69%	87.34%	85.40%	83.13%
		Test set	0.885(95% CI, 0.822–0.940)	82.31%	87.30%	77.61%	78.57%	86.67%
	Radiomics	Training set	0.723(95% CI, 0.670–0.769)	60.06%	87.72%	54.03%	29.63%	95.03%
		Test set	0.688(95% CI, 0.591–0.767)	54.61%	96.00%	44.76%	29.27%	97.91%
PPH	Clinical	Training set	0.884(95% CI, 0.833–0.927)	85.15%	63.63%	89.92%	58.33%	91.77%
		Test set	0.860(95% CI, 0.777–0.933)	81.13%	68%	84.76%	51.52%	91.75%
	Clinical-radiomics	Training set	0.918(95% CI, 0.881–0.948)	87.13%	50.91%	95.16%	70.00%	89.73%
		Test set	0.905(95% CI, 0.843–0.955)	84.61%	64%	89.52%	59.26%	91.26%

Note: PAS placenta accreta spectrum, PPH postpartum haemorrhage, PPV positive predictive value, NPV negative predictive value, AUC area under the curve

in good agreement with the actual clinical results. The clinical-radiomics model improved the prediction accuracy by combining critical clinical and radiomic data and enhancing its utility and operability in the clinical setting

by applying nomograms, decision curves, and calibration curve analysis. These methods provide clinicians with a valuable tool to more effectively assess and manage PAS and its associated risks.

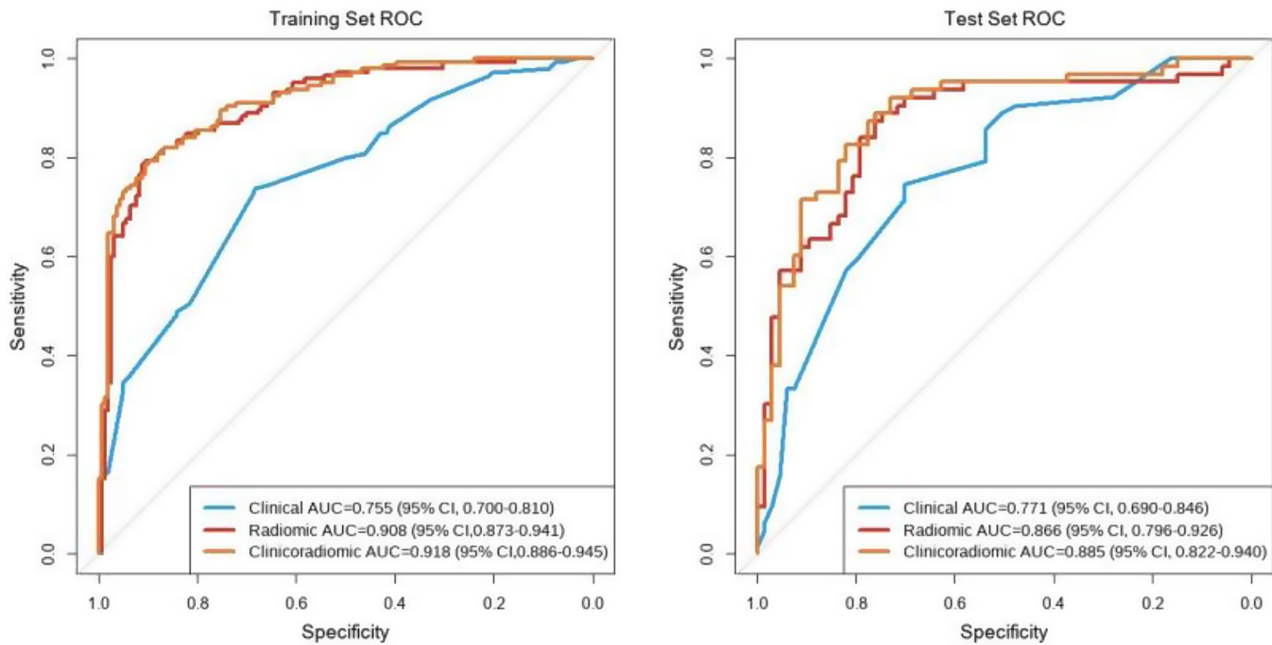


Fig. 5 ROC curve of the clinical, radiomics, and clinical-radiomics models for predicting PAS. Among the three models, the clinical-radiomics model demonstrated the best performance, with an AUC of 0.918 in the training set and an AUC of 0.885 in the test set

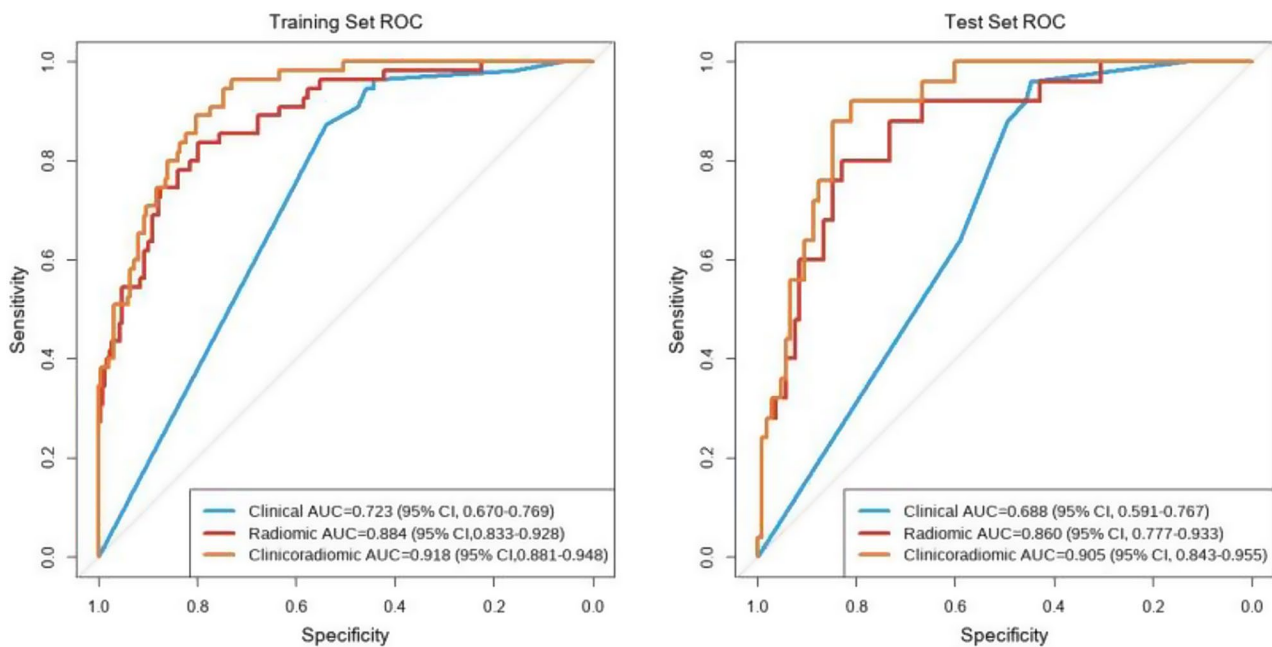


Fig. 6 ROC curves of the clinical, radiomics, and clinical-radiomics models for predicting the risk of PPH. Among the three models, the clinical-radiomics model demonstrated the best performance, with an AUC of 0.918 in the training set and an AUC of 0.905 in the test set

Discussion

This study constructed clinical, radiomics, and clinical-radiomics models to predict PAS and PPH risks, utilizing clinical data and radiomic features derived from T2WI. For the three models predicting PAS, the AUCs for the training set were 0.918, 0.908, and 0.755, and for the test set, the AUCs were 0.885, 0.866, and 0.771, respectively.

The results indicate that the clinical-radiomics model, integrating clinical independent risk factors and the R-score, outperformed individual radiomics and clinical models in antenatal PAS prediction. For the three models predicting PPH risk, the AUCs for the training set were 0.918, 0.884, and 0.723, and for the test set, the AUCs were 0.905, 0.860, and 0.688. Similarly, the

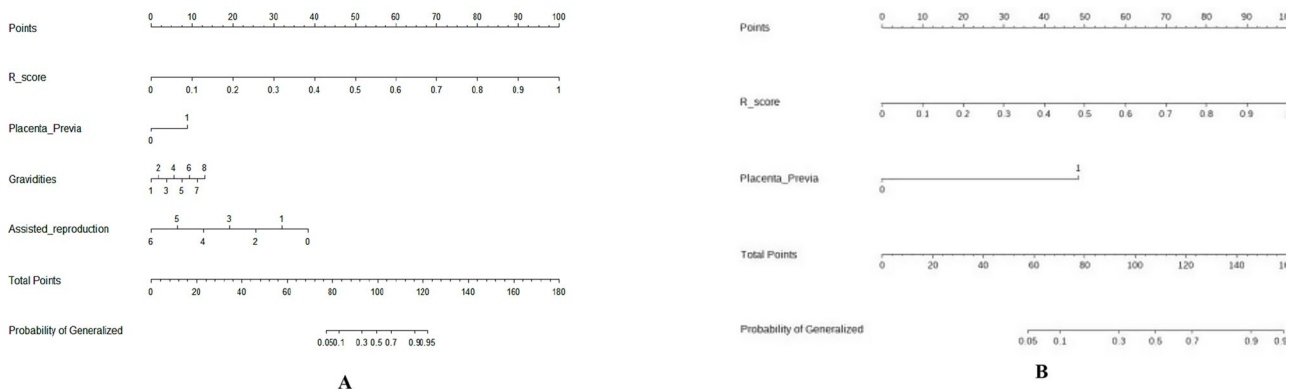


Fig. 7 (A) Clinical-radiomics model nomogram for predicting PAS. (B) Clinical-radiomics model nomogram for predicting the risk of PPH

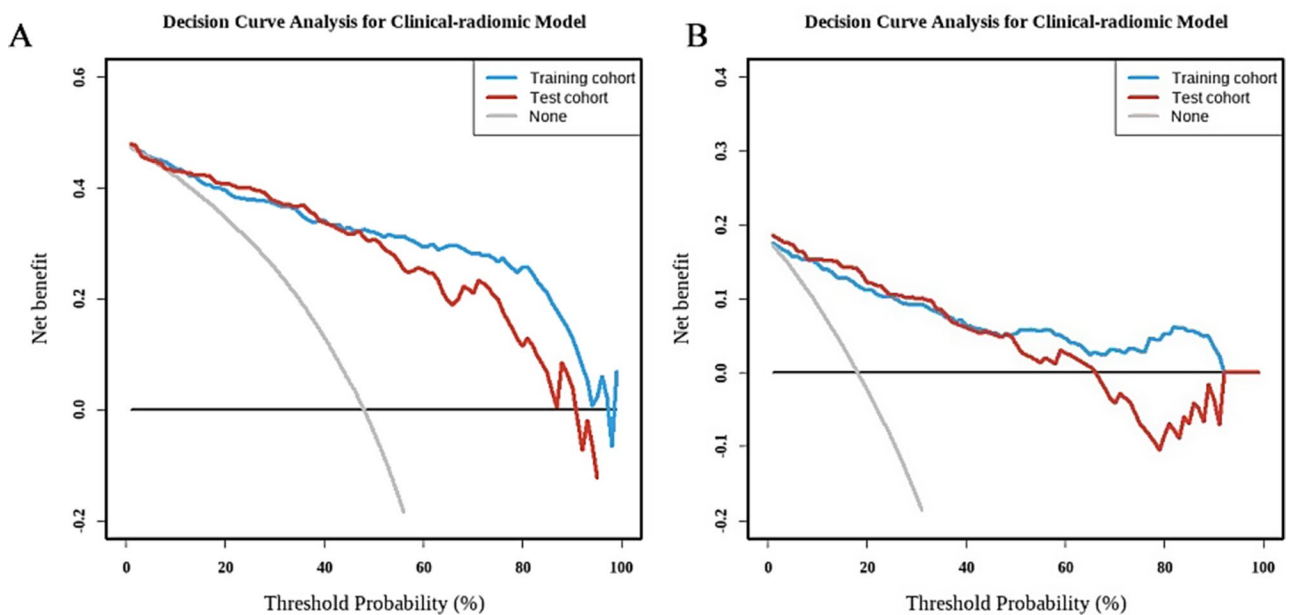


Fig. 8 (A) Clinical-radiomics model decision curves predicting PAS. (B) Clinical-radiomics model decision curves predicting the risk of PPH. The x-axis displays the threshold probability, and the y-axis measures the net benefit. The blue line represents the training set. The red line represents the test set, the gray line represents the assumption that all patients have PAS or PPH, and the black line represents the assumption that no patients have PAS or PPH

clinical-radiomics model outperformed the radiomics and clinical models in predicting PPH risk. Our findings demonstrate that the clinical-radiomics model, integrating the R-score and clinical factors, offers superior predictive performance compared to the radiomics model and significant advantages over the clinical model. These findings underscore the potential of radiomics models for predicting PAS and PPH risks, particularly in identifying pathological features, complemented by the important role of clinical factors in disease prediction.

MRI and Ultrasound are valuable for PAS diagnosis during pregnancy, and radiomics analysis based on these modalities demonstrates strong potential for PAS prediction [26–28]. Furthermore, studies have shown that the occurrence of PAS is closely related to maternal factors such as parity and placenta previa. Peng et al. [23]

developed an MRI-radiomics-clinical nomogram that integrates clinical factors, including placenta previa and prior uterine surgery, to effectively predict PAS. Zhao et al. [29]’s research also explored the incidence of suspected PAS and its potential risk factors, finding that more than three pregnancies, a history of cesarean section, and the presence of placenta previa significantly increased the likelihood of antenatal diagnosis of PAS. In our study, we also included parity and placenta previa as independent risk factors for PAS, consistent with these findings. Additionally, our study found a significant association between assisted reproduction and PAS. There is relatively less research on predicting PPH. Wu et al. [30] proposed an MRI-based clinical-radiomics nomogram for PPH prediction. In their study, the model achieved AUCs of 0.888 and 0.832 in the training and validation

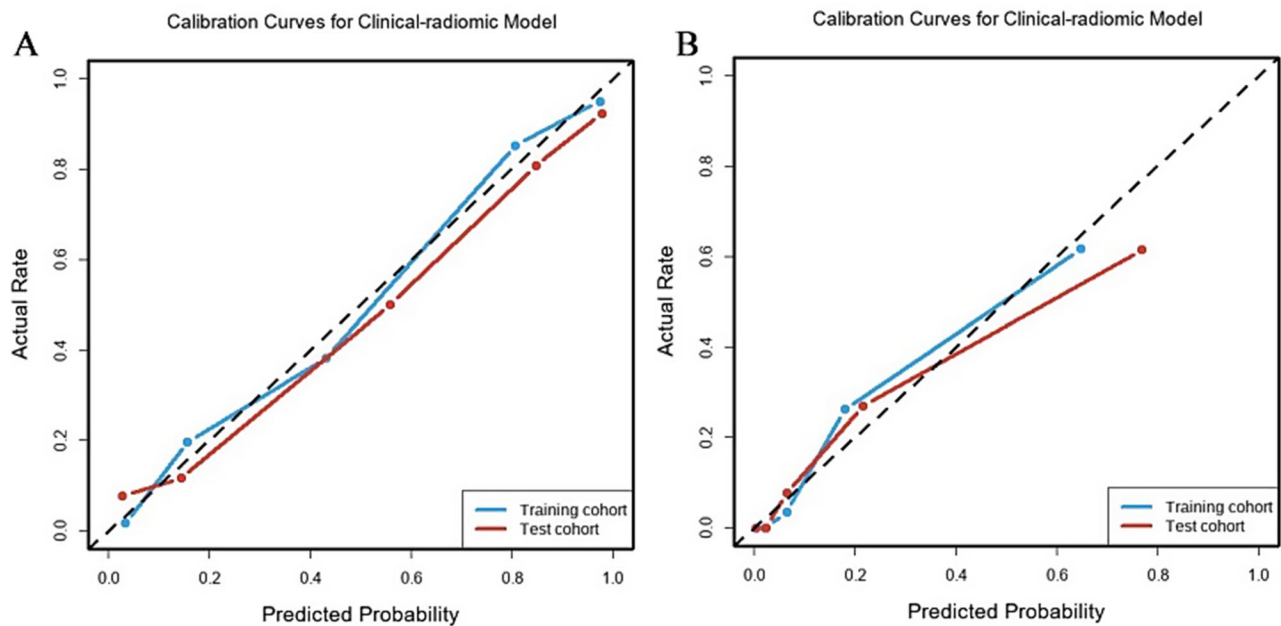


Fig. 9 (A) Calibration curves of the clinical-radiomics model predicting PAS. (B) The clinical-radiomics model predicting the risk of PPH. The x-axis represents the probability of PAS or PPH calculated by the clinical-radiomics model, and the y-axis represents the actual PAS or PPH incidence rate. The dotted diagonal line represents the perfect estimation by an ideal model, where the predicted outcomes perfectly correspond to the actual outcomes. The blue solid line represents the performance of the clinical-radiomics model in the training set. The red solid line represents the performance of the clinical-radiomics model in the test set. The closer the alignment of the solid lines with the dotted diagonal line, the more accurate the model's estimation

sets, respectively. In comparison, our clinical-radiomics model showed superior performance in predicting PPH, with AUCs of 0.918 and 0.905 in the training and test sets. In both studies, the clinical-radiomics model showed significant improvement over the standalone radiomics model, indicating the important role of clinical factors in PPH prediction. Notably, our model demonstrated a more significant improvement, which may be closely related to the clinical factors we included. Specifically, we incorporated “placenta previa” as a factor in our model. Previous studies have pointed out that placenta previa is an important factor in predicting PPH. For example, Lee et al. [31] demonstrated that placenta previa is a critical predictive factor in their scoring model for massive PPH in pregnancies. This factor is considered to be a primary driver underlying the enhanced performance of our model.

This study selected 43 radiomic features related to PAS, covering texture features, shape features, and wavelet transform features. Similar to previous studies, we also focused on commonly used radiomic features for analyzing texture details and detecting tissue heterogeneity, particularly the Gray Level Co-occurrence Matrix (GLCM) and Gray Level Size Zone Matrix (GLSZM). GLCM quantifies the spatial relationship between pairs of pixels in an image and extracts texture features such as contrast and roughness. In PAS, abnormal attachment and invasion of the placenta are often associated with tissue heterogeneity, and GLCM can capture these subtle

structural changes, helping us assess the risk of placental invasion into the myometrium. The model leverages the well-established advantages of these features in tissue anomaly detection, providing a solid foundation for PAS prediction. Currently, most related studies use a limited number of radiomic features, focusing mainly on texture and shape features. For example, Zhu et al. [21] proposed an MRI-based radiomics model for automatic PAS diagnosis combined with clinical features, which included 3 texture features and 3 shape features. The radiomics model achieved AUCs of 0.792 and 0.790 for the training and testing sets, respectively. Peng et al. [23] constructed a clinical-radiomics nomogram based on MRI, which included only 3 features: 2 texture features and 1 shape feature. The radiomics model achieved AUCs of 0.78, 0.81, and 0.75 for the training, independent validation, and external validation sets, respectively. Yu et al. [32] developed an MRI-based T2WI radiomics-clinical nomogram, incorporating 6 features. The radiomics model achieved AUCs of 0.803 and 0.780 for the training and validation sets, respectively. Compared to these studies, our model incorporated 43 radiomics features, covering various feature types, and achieved AUCs of 0.908 and 0.866 for the training and testing sets, respectively, demonstrating a significant improvement in performance. This enhancement is likely closely related to the selection of a greater number of features that are more relevant to the target variable, thereby boosting the model's predictive ability.

In the radiomics model for predicting PPH risk, features derived from wavelet transform play a key role, consistent with previous studies. For example, Wu et al. [30] constructed a clinical-radiomics nomogram based on MRI for predicting PPH, incorporating 35 features, more than half of which were obtained through wavelet transform. The radiomics model achieved AUCs of 0.876 and 0.795 for the training and validation sets, respectively. Our model achieved AUCs of 0.884 and 0.860 for the training and testing sets, respectively. Both models demonstrated impressive performance in predicting PPH. It is evident that wavelet-derived features are strongly associated with the occurrence of PPH. For instance, in this study, the three most important wavelet-based features in our model, wavelet-LLL_gldm_SmallDependenceHighGrayLevelEmphasis, wavelet-LLL_glszm_GrayLevelNonUniformity, and wavelet-HHL_glszm_SizeZoneNonUniformity, reflect the non-uniformity of different gray-level regions and texture structures in the image. These features capture subtle structural changes within the placental area, such as vascular morphology and tissue density, which may serve as potential indicators for the occurrence of PPH.

According to the current expert consensus guidelines, signs of MRI abnormality in PAS include thick low T2 signal bands within the placenta, placenta/uterus bulge, localized exophytic mass, thinning of the myometrium, interruption of the bladder wall, and ectopic blood vessels in the placenta bed [33–35]. When the placenta adheres to the myometrium, implants, or even penetrates the plasma membrane, it can entangle and pull with the local myometrium, thus causing morphological and signal changes in the placenta on MRI. These changes are not limited to the adhesion implantation or the lower uterine segment. Therefore, in this study, we selected sagittal T2WI of all the placenta (including the myometrium) to extract image features by outlining the ROI layer by layer.

This study could help clinicians reduce serious maternal complications and provide timely treatment in the event of serious complications. Most current studies have been limited to predicting PAS antenatally but have not focused on PPH. However, maternal hemorrhage during or after delivery is an important challenge in obstetric emergencies, where one of the keys to timely treatment is the accurate prediction and estimation of the amount of maternal hemorrhage during or after delivery during the antenatal period, underestimation of which may result in the loss of the opportunity for resuscitation. It has been reported that patients with placenta accreta, placenta increta, or placenta percreta are at increased risk of PPH [36–38]. However, in clinical practice, many pregnant women with non-PAS still tend to suffer from hemorrhage at the time of delivery, which can seriously

endanger the life of the mother and child. At the same time, some women with PAS also experience only a small amount of hemorrhage at the time of delivery. This study can help overcome this gap, assisting in the accurate prediction of PPH in non-PAS pregnant women clinically suspected of having PAS and in PAS pregnant women whose PAS prediction model failed to accurately predict hemorrhage, as this could help us identify pregnant women at high risk of PPH at an early stage, optimize the surgical management, proactively prevent perinatal complications, and improve the outcomes of mothers and babies.

This study has a few limitations. First, this was a retrospective single-center study, which may lead to selection bias and affect the generalizability of the results. Second, there is a potential bias in collecting non-consecutive patients and identifying positive and negative cases separately. Third, the invasive area of PAS was not evaluated, which may limit the comprehensive assessment of disease severity and its clinical implications. Fourth, although the models built in the study performed well on the training and test sets, their external validation and generalization capabilities still need to be confirmed by evaluating them on independent samples from different regions. Fifth, despite the robust performance of MRI in this study, its widespread adoption for screening may be limited by factors such as high costs, restricted accessibility, and the need for specialized expertise in image interpretation. Sixth, the study was conducted in a high-risk pregnancy cohort, potentially limiting the generalizability of the findings to the general pregnant population. Future research is planned to be carried out in the following aspects: first, we will actively seek cooperation with other medical institutions to establish a multi-center imaging data sharing platform, expand the scale and diversity of data, and improve the generalization ability of the model. Second, we will continuously optimize the algorithms and parameters of the radiomics model to enhance its accuracy and stability. In addition to validating single-center retrospective data, multi-center prospective studies should also be conducted to further verify the robustness of the model. Finally, the findings of this study could be integrated with information from other imaging modalities (other magnetic resonance sequences and ultrasound examinations), pathology, and other multi-disciplinary information to further improve the accuracy and effectiveness of the clinical-radiological model in predicting the risks of PAS and PPH antenatally.

Conclusion

Radiomics analysis based on MRI T2WI suggests potential for the antenatal prediction of PAS and PPH risks. The clinical-radiomics model, which integrates high-dimensional imaging features with independent clinical

risk factors, appears to offer improved predictive performance compared to standalone radiomics and clinical models, potentially surpassing existing MRI-based approaches in accuracy. However, the generalizability of our findings may be constrained by the single-center nature of the data and the absence of multicenter validation. Future studies should prioritize multicenter collaborations and external validation to evaluate the model's robustness and applicability across diverse clinical populations.

Abbreviations

PAS	Placenta accreta spectrum
PA	Placenta accreta
PI	Placenta increta
PP	Placenta percreta
PPH	Postpartum hemorrhage
MRI	Magnetic resonance imaging
T2WI	T2-Weighted imaging
ROI	Region of interest
ICC	Class correlation coefficient
LASSO	Least Absolute Shrinkage and Selection Operator
PPV	Predictive Value
NPV	Negative Predictive Value
AUC	Area Under the Receiver Operating Characteristic Curve

Supplementary Information

The online version contains supplementary material available at <https://doi.org/10.1186/s12884-025-07516-0>.

Supplementary Material 1

Acknowledgements

We thank the participants and clinical site staff for their contributions to this study.

Author contributions

JL Z: data curation, MRI reading and segmentation, statistics, writing of original draft WW: radiomic analysis, methodology, project administration, supervision YZ X: radiomic analysis, statistics, writing of original draft XLW: MRI reading, supervision, review and editing KY W: supervision, review and editing LZ X: review and editing YT L: Conceptualization, project administration, MRI reading, review and editing.

Funding

This study was supported by the Capital's Funds for Health Improvement and Research (NO.2022-2-2117), Natural Science Basic Research Program of Shanxi (No.2023-JC-YB-682), and National Natural Science Foundation of China (No. 82371936) in study design and analysis of data.

Data availability

The datasets generated and/or analysed during the current study are not publicly available due privacy or ethical restrictions but are available from the corresponding author on reasonable request.

Declarations

Ethics approval and consent to participate

This retrospective study was approved by the Ethics Committee of Beijing Obstetrics and Gynecology Hospital, Affiliated with Capital Medical University (approval number: 2022-KY-049-01). The study was conducted according to the principles of the Declaration of Helsinki. The Ethics Committee of Beijing Obstetrics and Gynecology Hospital, Affiliated with Capital Medical University, has waived the need for informed consent.

Consent for publication

Written informed consent for publication was obtained.

Competing interests

The authors declare no competing interests.

Author details

¹Department of Radiology, Beijing Obstetrics and Gynecology Hospital, Capital Medical University, Beijing Maternal and Child Health Care Hospital, 17 Qihelou Street, Dongcheng District, Beijing 100006, China
²School of Electronics and Information, Xi'an Polytechnic University, Shaanxi, China
³GE Healthcare, Beijing, China

Received: 27 September 2024 / Accepted: 24 March 2025

Published online: 04 April 2025

References

- Brown LA, Menendez-bobseine M. Placenta accreta spectrum. *J Midwifery Women's Health*. 2021;66(2):265–9. <https://doi.org/10.1111/jmwh.12811>
- Neary C, Naheed S, McLernon DJ, Black M. Predicting risk of postpartum haemorrhage: a systematic review[J/OL]. *BJOG: Int J Obstet Gynecol*. 2021;128(1):46–53. <https://doi.org/10.1111/1471-0528.16379>
- Baldwin HJ, Nippita TA, Torvaldsen S, Lbiebele L, Ford JB, Patterson A JA. Outcomes of subsequent births after placenta accreta spectrum. *Obstet Gynecol*. 2020;136(4):745–55. <https://doi.org/10.1097/AOG.0000000000004051>
- Silver RM, Branch DW. Placenta accreta spectrum. *N Engl J Med*. 2018;378(16):1529–36. <https://doi.org/10.1056/NEJMc1709324>
- Einerson BD, Gilner JB, Zuckerwise LC. Placenta accreta spectrum. *Obstet Gynecol*. 2023;142(1):31–50. <https://doi.org/10.1097/AOG.0000000000005229>
- Giouleka S, Tsakiridis L, Kalogiannidis L, et al. Postpartum hemorrhage: A comprehensive review of guidelines. *Obstet Gynecol Surv*. 2022;77(11):665–82. <https://doi.org/10.1097/OGX.0000000000001061>
- Bailit JL, Grobman WA, Rice MM, et al. Morbidly adherent placenta treatments and outcomes. *Obstet Gynecol*. 2015;125(3):683–9. <https://doi.org/10.1097/AOG.0000000000000680>
- Fitzpatrick KE, Sellers S, Spark P, Kurinczuk JJ, Brockrehurst P, Knight M. The management and outcomes of placenta accreta, increta, and percreta in the UK: A population-based descriptive study. *BJOG*. 2014;121(1):62–71. <https://doi.org/10.1111/1471-0528.12405>
- Thurn L, Lindqvist PG, Jakobsson M, et al. Abnormally invasive placenta-prevalence, risk factors and antenatal suspicion: results from a large population-based pregnancy cohort study in the nordic countries. *BJOG*. 2016;123(8):1348–55. <https://doi.org/10.1111/1471-0528.13547>
- Baumann HE, Pawlik LKA, Hoelsli I et al. Accuracy of ultrasound for the detection of placenta accreta spectrum in a universal screening population. *Int J Gynaecol Obstet* 2023, 161(3):920–6. <https://doi.org/10.1002/ijgo.14595>
- American College of Obstetricians and Gynecologists. Society for Maternal-Fetal Medicine 2018 Obstetric care consensus 7: placenta accreta spectrum. *Obstet Gynecol* 132 6 e259–75 <https://doi.org/10.1097/AOG.0000000000000983>
- Fratelli N, Prefumo F, Maggi C, et al. Third-trimester ultrasound for antenatal diagnosis of placenta accreta spectrum in women with placenta previa: results from the ADoPAD study. *Ultrasound Obstet Gynecol*. 2022;60(3):381–9. <https://doi.org/10.1002/uog.24889>
- Patel-Lippmann KK, Planz VB, Phillips CH, Zuckerwise LC, Moshiri M. Placenta accreta spectrum disorders: update and pictorial review of the SAR-ESUR joint consensus statement for MRI. *Radiographics*. 2023;43(5):e220090. <https://doi.org/10.1148/rg.220090>
- Kapoor H, Hanaoka M, Dawkins A, Khurana A. Review of MRI imaging for placenta accreta spectrum: pathophysiologic insights, imaging signs, and recent developments. *Placenta*. 2021;104:31–9. <https://doi.org/10.1016/j.placenta.2020.11.004>
- Liu Q, Zhou W, Yan Z, et al. Development and validation of MRI-based scoring models for predicting placental invasiveness in high-risk women for placenta accreta spectrum. *Eur Radiol*. 2024;34(2):957–69. <https://doi.org/10.1007/s00330-023-10058-8>

16. Zagal AA, Hussian HK, Berjawi GA. MRI evaluation of the placenta from normal variants to abnormalities of implantation and malignancies. *J Magn Reson Imaging*. 2019;50(6):1702–17. <https://doi.org/10.1002/jmri.26764>.
17. Mar WA, Berggruen S, Atueyi U et al. Ultrasound imaging of placenta accreta with MR correlation. *Ultrasound Q*, 2015, 31(1):23–33. <https://doi.org/10.1097/RUQ.0000000000000127>
18. Nam D, Chapiro J, Paradis V, Seraphin TP, Kather JN. Artificial intelligence in liver diseases: improving diagnostics, prognostics and response prediction. *JHEP Rep*. 2022;4(4):100443. <https://doi.org/10.1016/j.jhepr.2022.100443>.
19. Guiot J, Vaidyanathan A, Deprez L, et al. A review in radiomics: making personalized medicine a reality via routine imaging. *Med Res Rev*. 2022;42(1):426–40. <https://doi.org/10.1002/med.21846>.
20. Nazari M, Shiri I, Zaidi H. Radiomics-based machine learning model to predict risk of death within 5-years in clear cell renal cell carcinoma patients. *Comput Biol Med*. 2021;129:104135. <https://doi.org/10.1016/j.combiomed.2020.104135>.
21. Zhu H, Yin X, Wang H, et al. A computerized diagnostic model for automatically evaluating placenta accreta spectrum disorders based on the combined MR radiomics-clinical signatures. *Sci Rep*. 2022;12(1):10130. <https://doi.org/10.1038/s41598-022-14454-w>.
22. Do QN, Lewis MA, Xi Y, et al. MRI of the placenta accreta spectrum (PAS) disorder: radiomics analysis correlates with surgical and pathological outcome. *J Magn Reson Imaging*. 2020;51(3):936–46. <https://doi.org/10.1002/jmri.26883>.
23. Peng L, Zhang X, Liu J, et al. MRI-radiomics-clinical-based nomogram for prenatal prediction of the placenta accreta spectrum disorders. *Eur Radiol*. 2022;32(11):7532–43. <https://doi.org/10.1007/s00330-022-08821-4>.
24. Peng L, Yang Z, Liu J, et al. Prenatal diagnosis of placenta accreta spectrum disorders: deep learning radiomics of pelvic MRI. *J Magn Reson Imaging*. 2024;59(2):496–509. <https://doi.org/10.1002/jmri.28787>.
25. Jauniaux E, Ayres-de-Campos D, Langhoff-Roos J, et al., et al. FIGO classification for the clinical diagnosis of placenta accreta spectrum disorders. *Int J Gynaecol Obstet*. 2019;146(1):20–4. <https://doi.org/10.1002/ijgo.12761>.
26. Sun H, Qu H, Chen L, et al. Identification of suspicious invasive placentation based on clinical MRI data using textural features and automated machine learning. *Eur Radiol*. 2019;29(11):6152–62. <https://doi.org/10.1007/s00330-019-06372-9>.
27. Young D, Khan N, Hobson SR, Sussman D. Diagnosis of placenta accreta spectrum using ultrasound texture feature fusion and machine learning. *Comput Biol Med* 2024, 178:10875710.1016/j.combiomed.2024.108757
28. AbdelAziz S, El-Goly NA, Maged AM, Bassiouny N, El-Demiry N, Shamel AJM-FM. Diagnostic accuracy of magnetic resonance imaging in the diagnosis of placenta accreta spectrum: A systematic review and Meta-analysis. *Maternal Fetal Med*. 2025;7(01):15–21.
29. Zhao J, Li Q, Liao E, et al. Incidence, risk factors and maternal outcomes of unsuspected placenta accreta spectrum disorders: a retrospective cohort study. *BMC Pregnancy Childbirth*. 2024;24(1):76. <https://doi.org/10.1186/s12884-024-06254-z>.
30. Wu Q, Yao K, Liu Z, et al. Radiomics analysis of placenta on T2WI facilitates prediction of postpartum haemorrhage: A multicentre study. *EBioMedicine*. 2019;50:355–65. <https://doi.org/10.1016/j.ebiom.2019.11.010>.
31. Lee JY, Ahn EH, Kang S, et al. Scoring model to predict massive post-partum bleeding in pregnancies with placenta previa: A retrospective cohort study. *J Obstet Gynaecol Res*. 2018;44(1):54–60. <https://doi.org/10.1111/jog.13480>.
32. Yu H, Yin H, Zhang H, Zhang J, Yue Y, Lu Y. Placental T2WI MRI-based radiomics-clinical nomogram predicts suspicious placenta accreta spectrum in patients with placenta previa. *BMC Med Imaging*. 2024;24(1):146. <https://doi.org/10.1186/s12880-024-01328-y>.
33. Familiari A, Liberati M, Lim P, et al. Diagnostic accuracy of magnetic resonance imaging in detecting the severity of abnormal invasive placenta: a systematic review and meta-analysis. *Acta Obstet Gynecol Scand*. 2018;97(5):507–20. <https://doi.org/10.1111/aogs.13258>.
34. Bourgioti C, Zafeiropoulou K, Fotopoulos S, et al. MRI features predictive of invasive placenta with extrauterine spread in High-Risk gravid patients: A prospective evaluation. *AJR Am J Roentgenol*. 2018;211(3):701–11. <https://doi.org/10.2214/AJR.17.19303>.
35. Jha P, Pöder L, Bourgioti C. Society of abdominal radiology (SAR) and European society of urogenital radiology (ESUR) joint consensus statement for MR imaging of placenta accreta spectrum disorders[J/OL]. *Eur Radiol*. 2020;30(5):2604–15. <https://doi.org/10.1007/s00330-019-06617-7>.
36. Kawakita T, Mokhtari N, Huang JC, Landy HJ. Evaluation of Risk-Assessment tools for severe postpartum hemorrhage in women undergoing Cesarean delivery. *Obstet Gynecol*. 2019;134(6):1308–16. <https://doi.org/10.1097/AOG.0000000000003574>.
37. Jauniaux E, Collins S, Burton GJ. Placenta accreta spectrum: pathophysiology and evidence-based anatomy for prenatal ultrasound imaging. *Am J Obstet Gynecol*. 2018;218(1):75–87. <https://doi.org/10.1016/j.ajog.2017.05.067>.
38. Lee C, Liao Z, Li Y, et al. Placental MRI segmentation based on multi-receptive field and mixed attention separation mechanism. *Comput Methods Programs Biomed*. 2023;242:107699doi. <https://doi.org/10.1016/j.cmpb.2023.107699>.

Publisher's note

Springer Nature remains neutral with regard to jurisdictional claims in published maps and institutional affiliations.